Research Square

Preprints are preliminary reports that have not undergone peer review.
They should not be considered conclusive, used to inform clinical practice,
or referenced by the media as validated information.

Groundwater level fluctuations in coastal aquifer: Using artificial neural networks to predict the impacts of climatical CMIP6 scenarios

Adib Roshani
Babol Noshirvani University of Technology
Mehdi Hamidi (Hamidi@nit.ac.ir)
Babol Noshirvani University of Technology https://orcid.org/0000-0002-7376-3303

Research Article

Keywords: CMIP6, Groundwater level, Artificial neural network, LARS-WG, Sari-Neka

Posted Date: March 9th, 2022

DOI: https://doi.org/10.21203/rs.3.rs-1403266/v1

License: This work is licensed under a Creative Commons Attribution 4.0 International License. Read Full License

Abstract

The groundwater resources play a crucial role in satisfying water for use in domestic, industrial, and agricultural applications. The aim of this study was to investigate the changes in groundwater level in the Sari-Neka coastal aquifer near the Caspian Sea in Iran by ANN based on the emission scenarios of the sixth IPCC report for the next two decades. Three models selected from Coupled Model Intercomparison Project Phase 6 (CMIP6), including ACCESS-CM2, HadGEM3-GC31-LL, and NESM3, are validated. The result shows that ACCESS-CM2 had the best performance, and by using LARS-WG simulation, the temperature and precipitation were done based on two emission scenarios, SSP2-4.5 and SSp5-8.5, during 2021-2040. In addition, the K-means method used for clustering, and the Elbow method was utilized to select the optimal number of piezometers. In the following, the monthly maximum and minimum temperature, precipitation, and water table of previous month from 4 observation piezometers are used as input variables to forecast the groundwater level in the forthcoming months. The results of r, R^2, RMSE, and MAE are evaluated for the model and indicate the good performance of the model. The results imply that under such mentioned scenarios, the mean monthly temperature will rise approximately 0.1-1.2 °C; also, the mean monthly precipitation will witness changes from -10% to 78% in the next two decades. As a result, this is likely to lead to improvement and recharge of groundwater level for the near future. The results can help managers and policymakers to identify adaptation strategies more precisely for basins with similar climates.

1 Introduction

According to studies by the Intergovernmental Panel on Climate Change (IPCC), the shortage of water resources is expected to become a major challenge in many regions of Asia as the demand for water increases due to a rise in population and standards of living (IPCC 2014). Given the strong dependence of the Asian economy on agriculture, about 80% of groundwater in Asia is used for this purpose. The groundwater level in coastal locations can be influenced by tides, increased seawater level, increased salinity, uncontrolled withdrawal, and reduced recharge (Hamidi and Sabbagh-Yazdi 2008; Natarajan and Sudheer 2020; Nasiri et al. 2021). As an arid and semi-arid country in Western Asia, Iran has a shoreline of 750 km on the Caspian Sea and about 2250 km on the Persian Gulf and the Gulf of Oman, and numerous islands and estuaries, hence earning the title of a coastal country. As of the latest census, about 22% of Iran's population inhabit coastal lines. These regions play a significant role in the economic growth of a developing society, in terms of both agriculture and industry. Moreover, they can greatly contribute to the gross domestic product of a country. The critical role played by groundwater in this economic growth necessitates the awareness and management of changes in groundwater levels. Groundwater has come under threat in recent decades due to climate change and population growth. Researchers employ theoretical and observational models to investigate prospective climate conditions. General circulation models (GCMs) are some of the most authoritative theoretical models based on physics (O'Neill et al. 2017). However, they have certain disadvantages, such as their large scale. Nonetheless, they can be converted to small scales through some methods termed downscaling methods (Hewitson and Crane 1996; Wilby and Wigley 1997; Guo and Wang 2016). One of the most well-known and useful downscaling models is the Long Ashton Research Station-Weather Generator (LARS-WG) developed by Semenov and Barrow (Semenov et al. 1998). Its input data include minimum temperature, maximum temperature, precipitation, and sunshine hours or solar radiation on a daily scale. This model is capable of

simulating climatic parameters for future decades based on various scenarios and GCMs. The models in Coupled Model Intercomparison Project Phase 6 (CMIP6) have produced the latest simulations of the past, present, and future climates for a better understanding of climate change. The new models boast considerable improvements over those used in CMIP5, including a higher resolution and better physics (Priestley et al. 2020; Xin et al. 2020). Various researchers have simulated climatic parameters via the LARS-WG model and confirmed the results (Hassan et al. 2014; Sha et al. 2019; Bayatvarkeshi et al. 2020).

In recent years, an international body of climatologists and economists have created a wide range of new pathway scenarios, which describe changes in climate and the international community in terms of population, economy, and greenhouse gas (GHG) emission. The newest of these is named the Shared Socio-economic Pathways (SSP) and is divided into five categories, namely SSP1 to SSP5. These scenarios are displayed in the form of SSPx-y, where x represents the SSP, and y denotes the radiative forcing (w/m^2) in 2100 (O'Neill et al. 2016; Gupta et al. 2020).

The artificial neural network (ANN) is known as an estimator the effectiveness of which has been verified in previous research. It has been utilized in numerous scientific fields in recent years (Yoon et al. 2011; Shen et al. 2018; Rajaee et al. 2019). Its applications in hydrology include the prediction of nonlinear phenomena, such as rainfall-runoff, evapotranspiration, dam volume evaluation, streamlines, water and rain quality modeling (Taormina et al. 2012; Zhao et al. 2020; Roy et al. 2020; Di Nunno and Granata 2020; Chen et al. 2020; Derbela and Nouiri 2020). One of the most important challenges in forecasting groundwater levels via ANN has been the selection of input data. Daily, weekly, or monthly temperature and precipitation have been the major driving factors in the impact of climate change on water resources in the literature. (Yoon et al. 2011; Maharjan et al. 2021). Moghaddam et al. (2019) used monthly evaporation, average temperature, aquifer discharge and recharge, and aquifer level to evaluate the performance of ANN, Bayesian network (BN), and MODFLOW in the simulation of a 12-year period. Hasda et al. (2020) employed the neural network (NN) to forecast weekly levels of groundwater 52 weeks in advance. The studies by (Chang et al. 2015; Ghazi et al. 2021; Sharma et al. 2021) investigated the impact of climate change using the output of CMIP3 and CMIP5 climate models and various scenarios on variations in groundwater level.

Groups of climate model outputs have been utilized through coordination between different organizations to standardize the design of GCMs and the distribution of simulated models. They have recently become a crucial element in guiding global research on climate (Thorn et al. 2017). The rapid growth in population and industry has diverse effects on the manner of GHG emissions. New emission scenarios are introduced every couple of years. Hence, it is necessary to be up-to-date on the latest trends in climate change. The most common aim of climate studies is to determine the changes in the weather of the region under study, and most previous research has used CMIP3 or CMIP5 outputs for this purpose. However, the present study attempts to evaluate the best available models (CMIP6) for the specified basin. The main objective of the CMIP6 is to answer three vital questions of how the structure of the earth responds to different forces in relation to the origins and consequences of organized models, climate change quantification, and scenario uncertainty. The number of vertical layers in all CMIP6 models has been increased compared to those in CMIP5 models. An advantage of this increase is a more accurate simulation in the stratosphere. Also, the number of investigated prospective scenarios has significantly increased. The new scenarios added to CMIP6 are SSP1-1.9, SSP4-3.4, and SSP3-

7.0. In addition, the 4 scenarios SSP1-2.6, SSP2-4.5, SSP4-6.0, and SSP5-8.5 are updates on scenarios RCP2.6, RCP4.5, RCP6.0, and RCP8.5, respectively, in CMIP5 (Eyring et al. 2016; Li et al. 2020; Gupta et al. 2020).

The main aim of this research is to study atmospheric changes and forecast the monthly groundwater level of the coastal Sari-Neka aquifer in Iran via a NN under the latest scenarios codified by the Intergovernmental Panel on Climate Change (IPCC) (SSP2-4.5, SSP5-8.5) for future decades. The new CMIP6 models are enhanced in terms of horizontal resolution and better representation of synoptic processes (Di Luca et al. 2020; Nie et al. 2020; Srivastava et al. 2020), which will lead to more reasonable results in climate studies. So, the CMIP6 simulations of climate are more reliable than they were before.

2 Materials And Methods

2.1 study area

Sari-Neka region is a basin which is located by the Caspian Sea between (35° 56' 36° 52' N and 52° 43' 54° 44' E), is selected as a case study at the Mazandaran province (Fig. 1). It is divided into mountainous parts, hills, and flat plains, mainly covered by alluvial sediments from a geomorphological view. The Sari-Neka climate regard to the DeMartonne's method is generally Mediterranean and semi-humid. This region covers an area of about 6938.5 km^2, of which an area of 977.87 km^2 is devoted to the plains, while the rest is devoted to the highlands (5877.8 km^2). The highest elevation in the area is 3836 m, and the lowest point is -27 m (Nasiri et al. 2021). Annual average rainfall fluctuated between 400–1000 mm from 2000 to 2019 and the most humid months are related to October and November. Moreover, the mean maximum and minimum temperatures are 23 and 13 Celsius, respectively.

2.2 Date collection

Different datasets were prepared for this study that can be identified as:

1- Maximum temperature, minimum temperature, and precipitation data of historical and future period for three models ACCESS-CM2, HadGEM3-GC31-LL, and NESM3 under CMIP6 report from IPCC based on SSP2-4.5 and SSP5-8.5 scenarios were received for downscaling from https://climate4impact.eu.

2- Maximum and minimum temperatures, and precipitation for the observation period were provided from the meteorological organization of Mazandaran province on a daily scale.

3- Data on groundwater level fluctuations in 68 piezometers were provided from the regional water organization of Mazandaran province.

2.3 Climate models and emissions scenarios

In this study, the outputs of three climate models from CMIP6 were received from the mentioned databases, and the data of the region were extracted using ArcGis10.8. The ACCESS-CM2, HadGEM3-GC31-LL, and NESM3 models were used. The precipitation, maximum temperature, and minimum temperature of these models are available and presented in Table 1. The SSP2-4.5 and SSP5-8.5 scenarios were used for this study which are called The Middle of the road and Fossil-fueled development—Taking the highway, respectively. The specifications of scenarios are summarized in Table 2. The present study used these scenarios due to the

following reasons: (1) the SSP2-4.5 and SSP-5-8.5 are utilized for the vulnerabilities to climate change and its consequences (Warnatzsch and Reay 2019); (2) since SSP1-2.6, which is an update on RCP2.6, is absent in some models, a comparison between the models becomes problematic.

Table 1
List of CMIP6 models that have been used in this study (Priestley et al., 2020)

Model name	Institution	resolution	Processing	Simulated scenarios
ACCESS-CM2	CSIRO-ARCCSS; Commonwealth Scientific and Industrial Research Organization, and Bureau of Meteorology (Australia)	192*145	r1i1p1f1	SSP2-4.5 SSP5-8.5
HadGEM3-GC31-LL	MOHC; Met Office Hadley Center, United Kingdom	192*144	r1i1p1f1	SSP2-4.5 SSP5-8.5
NESM3	NUIST; Nanjing University of Information Science and Technology, China	192*96	r1i1p1f1	SSP2-4.5 SSP5-8.5

Table 2
Summary of assumptions regarding demographic and human development elements of SSP2 and SSP5 (O'Neill et al., 2017)

SSP element	SSP2	SSP5
Technology		
Development	Medium, uneven	Rapid
Carbon intensity	Medium	High
Energy tech change	Some investment in renewables but continued reliance on fossil fuels	Directed toward fossil fuels; alternative sources not actively pursued
Economy & lifestyle		
Growth (per capita)	Medium, uneven	High
Globalization	Semi-open globalized economy	Strongly globalized, increasingly connected
Consumption & Diet	Material-intensive consumption, medium meat consumption	Materialism, status consumption, tourism, mobility, meat-rich diets
Policies & institutions		
International Cooperation	Relatively weak	Effective in pursuit of development goals, more limited for envt. goals
Environmental Policy	Concern for local pollutants but only moderate success in implementation	Focus on local environment with obvious benefits to well-being, little concern with global problems
Policy orientation	Weak focus on sustainability	Toward development, free markets, human capita

2.4 Downscaling

Presently, GCM outputs are not directly employed in hydrological models due to their resolution inability and their lack of sufficient spatial and temporal certainty (Semenov and Barrow 1997). The model employed by this research is LARS-WG6, the initial version of which was introduced by Racsko et al. (1991) to address the issues of the Markov chain, which was frequently used to model precipitation, and later upgraded by Semenov and Barrow. As a generator, LARS-WG produces climatic parameters, such as maximum temperature, minimum temperature, precipitation, and solar radiation on a daily basis for any period of time according to a set of semi-empirical distributions. It must be noted that this model is not a weather forecast tool but a means to generate an artificial weather time series that statistically resembles observational data.

The delta change factor (DCF) technique was utilized to generate the Atmosphere-Ocean General Circulation Model (AOGCM) climate change scenario. This method calculates the maximum and minimum temperature difference and the precipitation ratio of the prospective and base periods in the studied region's model according to Eq. 1, 2, and 3. In this research, the base and prospective periods were taken to be 2000–2019 and 2021–2040, respectively (Semenov and Barrow 1997).

$$\Delta P_i = \bar{P}_{GCM,FUT,i} / \bar{P}_{GCM,Base,i} \quad (1)$$

$$\Delta T_{i,Min} = \bar{T}_{Min(GCM,FUT,i)} - \bar{T}_{Min(GCM,Base,i)} \quad (2)$$

$$\Delta T_{i,Max} = \bar{T}_{Max(GCM,FUT,i)} - \bar{T}_{Max(GCM,Base,i)} \quad (3)$$

In the above equations, ΔP_i, $\Delta T_{i,Min}$, and $\Delta T_{i,Max}$ represent the climate change scenarios of precipitation, minimum temperature, and maximum temperature, respectively, for every month. In addition, $\bar{P}_{GCM,FUT,i}$ denotes the 20-year precipitation average simulated by the AOGCM models for the prospective period, and $\bar{P}_{GCM,Base,i}$ is the same for the base period (2000–2019 in this study). Also, the explanations provided for the minimum and maximum temperature are accurate.

Two files were created to generate climatic data in the LARS-WG model and to downscale the GCM data for future periods. The first file describes past climatic behavior, while the other file contains climate change scenarios. The model is calibrated in the first step and then verified using statistical tests and a comparison of the graphs.

2.5 Clustering of observation well

Clustering is an unsupervised learning technique in which samples are categorized into similar groups with identical features. A common clustering method is the K-means, which MacQueen introduced in 1967 (MacQueen 1967). In this method, the number of clusters is predetermined. The number of clusters was validated using the common Elbow index, which is determined by Eq. (4) (Brusco and Steinley 2007). There were 68 piezometers in this basin; thus, clustering was performed to avoid over-complication of the model. The geographical coordinates and groundwater levels of the piezometers were used for clustering.

$$WCSS = \sum_{k=1}^{K} \sum_{i \in C_k} \sum_{v=1}^{V} \left(x_{iv} - \bar{x}_{vk} \right)^2 \quad (4)$$

Where Ck is the set of observations in the Kth and $\bar{x}_{vk}$ is the mean of variable v in cluster k. In this technique, the number of clusters is directly related to the Within-Cluster Sum of Square (WCSS), which is the sum of squared distance between each point and the centroid in a cluster. The vertical axis represents WCSS, while the horizontal axis represents the number of clusters. In this index, the number of clusters K begins from 1 and grows up to where the value of WCSS remains almost constant. It is worth noting that this value is largest at the first cluster.

2.6 Artificial neural network (ANN)

Artificial neural networks (ANN) are typically based on human nervous systems. In hydrological contexts, these heuristics are particularly appropriate for predicting and forecasting variables because they are capable of modeling nonlinear, nonstationary, and nongaussian processes. NNs train themselves to recognize patterns in data in order to be able to forecast the output of a future set of similar data. NNs are mostly divided into three general layers. The input layer is responsible for receiving data, the output layer contains forecast information, and the middle layers perform the necessary calculations (Maier and Dandy 1997; Daliakopoulos et al. 2005; Moghaddam et al. 2019). The inputs are multiplied by synaptic weights and delivered to the first hidden layer. In the hidden units, the weighted sum of inputs is transformed by a nonlinear activation function (Taormina et al. 2012).

NNs are either feedforward or recurrent. The present research utilized feedforward NNs and the sigmoid activation function. Furthermore, the Levenberg-Marquardt algorithm was employed to train the NN (Daliakopoulos et al. 2005; Derbela and Nouiri 2020). In feedforward networks, the input enters from the left, and the output exits from the right. Moreover, the number of input and output neurons are determined by the number of parameters in the network, and those of the hidden layer are determined via trial and error. The hidden layer is tasked with linking the input and output layers. Using this layer, the NN can extract nonlinear relationships from the data input to the model.

Training is aimed at reaching a state where the network is capable of correctly responding to training data in addition to similar non-training data. NN learning is either supervised or unsupervised, the former of which was used in the present study. In this approach, training is mostly performed using sample vectors of pairs, such that a specific output vector is assigned to each input vector. As this group of vectors is presented to the network, the weights are corrected according to the learning algorithm. This research used minimum and maximum temperature, precipitation in the current month, and groundwater level in the previous month as the input data and groundwater level in the current month as the output data (Coppola et al. 2005; Chitsazan et al. 2015; Moghaddam et al. 2019).

2.7 Performance criteria

Statistical methods for assessing the error between observational and predicted are used by correlation coefficients (r), coefficients of determination (R^2), Mean Absolute Error (MAE), and Root Mean Squared Error (RMSE).

$$r = \frac{n\left(\sum_{i=1}^{n} O_i P_i\right) - \left(\sum_{i=1}^{n} O_i\right) \cdot \left(\sum_{i=1}^{n} P_i\right)}{\sqrt{\left(n\sum_{i=1}^{n} O_i^2 - \left(\sum_{i=1}^{n} O_i\right)^2\right) \cdot \left(n\sum_{i=1}^{n} P_i^2 - \left(\sum_{i=1}^{n} P_i\right)^2\right)}} \quad (5)$$

$$R^2 = \frac{\left[\sum_{i=1}^{n} \left(O_i - \bar{O}_i\right) \cdot (P_i - \bar{P}_i)\right]^2}{\sum_{i=1}^{n} \left(O_i - \bar{O}_i\right)^2 \cdot \sum_{i=1}^{n} (P_i - \bar{P}_i)^2} \quad (6)$$

$$RMSE = \sqrt{\frac{\sum_{i=1}^{n} (P_i - O_i)^2}{n}} \quad (7)$$

$$MAE = \frac{\sum_{t=1}^{n} \left| P_i - O_i \right|}{n} \quad (8)$$

Where n is the total number of measured data, P_i & O_i are the predicted and observed value, respectively, and $\bar{O}_i$ & $\bar{P}_i$ are the averaged value of the measured data.

3 Result And Discussion

3.1 CMIP6 models validation

In the first step, the performances of the NESM3, HadGEM3-GC31-LL, and ACCESS-CM2 models with respect to the observational data were evaluated using the R^2 coefficient of determination and the root-mean-square error (RSME) for the minimum and maximum temperature and precipitation parameters in order to determine the best model for studying climate change in the area. According to the results presented in Table 3, the ACCESS-CM2 model had the smallest RMSE at the minimum and maximum temperatures and the best precipitation performance in both statistical tests. This indicates the superiority of this model over the other two in simulating the area under study. Hence, it was selected for investigating climate change in the research step.

Table 3
Statistical comparison of AOGCM models to select the best model

statistical test	Models AOGCM		
	Maximum temperature		
	ACCESS-CM2	HadGEM3-GC31-LL	NESM3
R^2	0.97	0.96	0.98
RMSE (°C)	4.09	6.32	5.19
	Minimum temperature		
	ACCESS-CM2	HadGEM3-GC31-LL	NESM3
R^2	0.98	0.95	0.98
RMSE (°C)	5.55	8.38	5.75
	precipitation		
	ACCESS-CM2	HadGEM3-GC31-LL	NESM3
R^2	0/95	0/94	0/94
RMSE (mm)	2.29	2.51	2.70

This step involved a forecast of the meteorological data by the ACCESS-CM2 model under the climate change scenarios SSP2-4.5 and SSP5-8.5. Additionally, the climatic data between 2000 and 2019 were utilized for the LARS-WG model's base period, and forecasts were made for the subsequent two decades (2021–2040). Calibration and verification were performed simultaneously using the Site Analysis functionality of the LARS-WG model and two datasets containing daily observational data and the geographical information of the research station. Moreover, the K-S, t, and F statistical tests were carried out to verify the performance of LARS-WG. The K-S test was conducted to test the equality of the seasonal distributions of the wet and dry series, the daily distribution of precipitation, and the daily distribution of minimum and maximum temperature. The F-test was performed to test the equality in the standard deviation of monthly precipitation, while the t-test was aimed at testing the equality of the monthly average of precipitation and the monthly average of the maximum and minimum daily temperature. The P-values calculated in all the tests indicated no significant difference between the observational and simulated values with a significance level of 5%. According to Table 4, the LARS-WG model exhibited acceptable consistency between the simulated and observational series of monthly climate data (Nover et al. 2016; Adnan et al. 2019). However, the same results were erroneous and reliable for a daily scale. In addition, the largest error corresponds to the simulated precipitation in January. The larger error for the precipitation compared to the other two parameters may be due to the large variation in precipitation (Hassan et al. 2014). Given the results of the model, the maximum temperature was simulated better than the other two parameters and possessed higher accuracy (Bayatvarkeshi et al. 2020). Although there is no complete correlation between the models and observations to date, the lack of quite correlation is not a barrier to the climate model's use. Climate models are not used to predict specific weather events; instead, they predict a trend in climate change over time (Warnatzsch and Reay 2019). Table 4 presents a statistical comparison between the simulated and observational values of the climatic parameters. The overall statistical evaluation of the ACCESS-CM2 model produced an acceptable result.

Table 4
K-S test daily distribution of observational and simulated data

Month	Minimum temperature			Maximum temperature			precipitation		
	evaluation	K-S	P-value	evaluation	K-S	P-value	evaluation	K-S	P-value
January	*	0.105	0.999	*	0.053	1.000	*	0.138	0.971
February	*	0.053	1.000	*	0.106	0.999	*	0.060	1.000
march	*	0.053	1.000	*	0.053	1.000	*	0.048	1.000
April	*	0.053	1.000	*	0.010	1.000	*	0.054	1.000
May	*	0.053	1.000	*	0.053	1.000	*	0.105	0.999
June	*	0.053	1.000	*	0.106	0.999	*	0.078	1.000
July	*	0.053	1.000	*	0.053	1.000	*	0.062	1.000
August	*	0.106	0.999	*	0.053	1.000	*	0.107	0.999
September	*	0.053	1.000	*	0.053	1.000	*	0.089	1.000
October	*	0.053	1.000	*	0.053	1.000	*	0.081	1.000
November	*	0.053	1.000	*	0.053	1.000	*	0.067	1.000
December	*	0.053	1.000	*	0.053	1.000	*	0.067	1.000

∗: not statistically significant

3.2 Future Climate modeling

Figure 2 displays a comparison of the average minimum and maximum temperatures of the base period and the average monthly temperature for both SSP2-4.5 and SSP5-8.5 scenarios during the 2021–2040 period. As shown in the figure, the minimum and maximum temperature in both scenarios will increase during all the months due to climate change and a rise in GHG. The scenarios forecast minimum and maximum temperature increases of 0.2°C to 1.3°C for the future. The largest increase in minimum temperature corresponds to SSP5-8.5 with a 1.3°C in November, and the smallest increase is in February (0.2°C), corresponding to SSP5-8.5. A similar procedure was carried out for maximum temperature, and the results indicated that the most significant changes relative to the base period will occur in April under SSP5-8.5, while the smallest will occur in October under SSP2-4.5. In general, it can be said that the average air temperature in this basin is on the rise. This increase in temperature may be due to the unstable and rapid industrial development in this region. The results of the present study are in good agreement with previous research by (Al-Maktoumi et al. 2018; Shahvari et al. 2019; Maghsood et al. 2019).

The average monthly precipitation during the base period and the forecast period (2021–2040) for both scenarios is displayed in Fig. 2. Except for February, May, June, and September, the results show an increase in precipitation for the rest of the months. The largest increase corresponds to the SSP5-8.5 scenario at 41 mm compared to the base period in October. On the other hand, the smallest increase corresponds to September at

6.3 mm under SSP2-4.5. In general, the precipitation forecast during the next two decades varies between −12% and 78% and the overall trend for 2000–2040 is increasing (Abiodun et al. 2017; Konapala et al. 2020; Tabari 2020). In addition, the results of Zhang et al. (2016), who studied 3 different GCMs under the RCP2.6, RCP4.5, and RCP8.5 scenarios, indicated that precipitation in the RCP2.6 and RCP4.5 scenarios increase gradually and continuously, but the increase in precipitation in future decades under RCP8.5 is remarkable.

The highest-precipitation month during the observational period was November, but it changes to October due to climate change in both scenarios. On the other hand, August remains the warmest month for the two coming decades. In addition, the results indicated that the highest increase in precipitation occurred in the winter and fall, while the largest absolute increase corresponds to July and August during the summer, which agrees with the results of Sha et al. (2019). The results indicated an increase in precipitation in both scenarios. According to IPCC, a rise in temperature intensifies the groundwater cycle and increases evaporation. In turn, an increase in evaporation leads to frequent and strong storms and may further humidify humid regions and dry out dryer regions. Moreover, according to the results of Boudiaf et al. (2020), the coastal Mediterranean regions have witnessed an increase in temperature and precipitation. Climate change has contributed to atmospheric warming and resulted in stronger precipitation. An increase in precipitation can lead to a higher snow potential in the heights, but a change in the form of precipitation, such as stronger precipitation, is encountered during the same period due to higher temperatures (Araya-Osses et al. 2020).

3.3 Clustering

The Elbow index was used in this paper to determine the optimal number of clusters. The outcome of the clustering is displayed in Fig. 3. The results indicated a significant difference in WCSS in the first 4 clusters. However, this difference becomes negligible from K = 4 onward; hence, 4 clusters were considered for the region under study. The locations of the 4 clusters and the 4 piezometers are shown in Fig. 4.

3.4 Groundwater modeling

The groundwater level of the Sari-Neka basin under climate change during the 2021–2040 period was predicted in MATLAB using NN. For this purpose, the data were divided into training, validation, and testing data. Moreover, 75% of the data were assigned to training, and 15% were assigned to validation and testing each. An important point in ANN is the number of neurons in the hidden layer. Trial and error resulted in an optimal number of 8 neurons. In the first step, the model was trained to simulate the groundwater level during the observational period. It was then used to predict the prospective groundwater level. The maximum temperature, minimum temperature, precipitation in the current month, and groundwater level in the previous month were used to develop the ANN model. Furthermore, the groundwater level in the current month was used for the output of the ANN model. The performance of the constructed model was assessed for all 4 piezometers clustered for the 2000–2019 period, with the results shown in Table 5. The findings indicated acceptable network performance at all 4 piezometers (Chitsazan et al. 2015; Sun et al. 2016; Derbela and Nouiri 2020).

Moreover, previous research results have demonstrated that the 3 available observational data inputs (groundwater level, temperature, and precipitation or evaporation) are sufficient to construct a high-performance NN (Daliakopoulos et al. 2005; Szidarovszky et al. 2007; Mohanty et al. 2010; Chang et al. 2015; Ghazi et al. 2021).

Table 5
Performance of the artificial neural network based on Correlation coefficient (r), coefficient of determination (R^2), root mean square error (RMSE) and Mean absolute error (MAE)

Representative cluster well	UTM_X	UTM_Y	r	R^2	RMSE(m)	MAE
P1	692,838	4,058,999	0.835	0.697	0.324	0.233
P2	697,350	4,075,550	0.929	0.864	0.360	0.253
P3	686,501	4,048,865	0.860	0.739	0.878	0.639
P4	688,031	4,074,145	0.895	0.802	0.339	0.237

The Taylor diagram was used for a better understanding of the results predicted by the NN (Fig. 5). In the Taylor diagram, the horizontal and vertical axes represent the observational data and the standard deviation, respectively. As the points approach the hypotenuse in this diagram, it becomes clear that the standard deviation of the predicted data is close to that of the observational data, validating the performance of the model. Furthermore, the correlation coefficient is on the main hypotenuse and measures the performance of the model on a 0-1 basis, where a value close to 1 indicates the good performance of the model.

The observational groundwater level in all the piezometers, except the 4th one, is increasing, which indicates an improvement in the groundwater depth. Also, the groundwater depth at all the piezometers decreases with a gentle slope in the coming two decades due to climate change (Chang et al. 2015). As seen from the observational trend of the four piezometers in Fig. 6, the depth of groundwater in the basin under study exhibits an increasing trend from about 2012 onward. However, a decreasing trend in depth due to climate change is observed for the coming two decades, except in the fourth piezometer under SSP2-4.5. As mentioned previously, given the higher precipitation in SSP5-8.5 compared to SSP2-4.5, the groundwater level in SSP5-8.5 will be higher than in the other scenario, and the largest change in the depth of groundwater corresponds to the piezometer P2 in SSP5-8.5. The results of previous research have demonstrated an increase in groundwater levels under climate change (Ligotin et al., 2010; Chang et al. 2015). One may conclude from the results that the groundwater level will improve in the future due to the influence of climatic parameters, such as temperature and precipitation. Nevertheless, other factors, such as industrial and economic developments, population growth, and migration, may adversely affect the availability of water resources.

4 Conclusions

Awareness of the changes in the groundwater level can make a remarkable contribution to water resource management. The present research investigated the effect of climate change on the groundwater level of the coastal Sari-Neka aquifer. In the first step, the 3 GCMs in the 6th IPCC report (AR6) along with the SSP2-4.5 and SSP5-8.5 scenarios were studied, and the best model was selected for the area. Subsequently, the weather parameters (temperature and precipitation) were simulated under the ACCESS-CM2 model for the coming two decades. The results have indicated that the selected model is an improvement over the previous ones, i.e., ACCESS 1.0 and ACCESS 1.3 (Williams et al. 2018; Bodman et al. 2020). To this end, the LARS-WG was employed for downscaling. The results indicated that the precipitation fluctuated between − 10–78% and average temperature (0.1–1.2°C) will increase, which agrees with other research results in this field (Tan et al. 2017; Anjum et al. 2019; Yan et al. 2019). Variations in precipitation throughout the months of the year can

make events such as floods and droughts more frequent, for which efficient strategies must be undertaken. In the second step, the 68 piezometers were clustered based on geographical coordinates and groundwater level and evaluated using the Elbow method. This resulted in 4 piezometer clusters. Furthermore, the sigmoid activation function and the Levenberg-Marquardt algorithm were employed to construct the ANN model, and the number of neurons in the hidden layer was determined using trial and error that resulted in the number of 8 neurons. In addition, the groundwater depth was predicted under the two mentioned scenarios (SSP2-4.5 & SSP5-8.5) for the near future 2021–2040 period. The results indicated that the groundwater depth of the Sari-Neka basin will decrease with a gentle slope.

Declarations

Author information

Affiliations

Adib Roshani

Master Student, Department of Civil Engineering, Babol Noshirvani University of Technology, Babol, Iran

Mehdi Hamidi

Associate Professor, Department of Civil Engineering, Babol Noshirvani University of Technology, Babol, Iran

Contributions

Adib Roshani: Conceptualization and design of the study, Acquisition of data, Analysis and/or interpretation of data, Methodology, Software, Validation, Drafting the manuscript

Mehdi Hamidi: Conceptualization and design of the study, Acquisition of data, Analysis and/or interpretation of data, Methodology, Software, Validation, Revising the manuscript critically for important intellectual content, Approval of the version of the manuscript to be published, Project administration, Supervision

Corresponding author

Correspondence to Mehdi Hamidi

Ethics declarations

Ethical Approval Authors agreed to the ethical approval needed to publish this manuscript.

Conflicts of Interest The authors declare that they have no conflict of interest.

Consent to Participate The authors declare their consent to participate in this work.

Consent to Publish The authors declare their consent to publication of this manuscript by “Water Resources Management” journal.

Competing Interests The authors declared that they have no conflicts of interest to this work.

Data Availability All GCM models are available online from: https://climate4impact.eu

Code availability ANN is commercial codes.

Funding The authors have not received support from any organization for the submitted work.

References

1. Abiodun BJ, Adegoke J, Abatan AA, Ibe CA, Egbebiyi TS, Engelbrecht F, Pinto I (2017) Potential impacts of climate change on extreme precipitation over four African coastal cities. Clim Change 143(3):399–413
2. Adnan RM, Liang Z, Trajkovic S, Zounemat-Kermani M, Li B, Kisi O (2019) Daily streamflow prediction using optimally pruned extreme learning machine. J Hydrol 577:123981
3. Anjum MN, Ding Y, Shangguan D (2019) Simulation of the projected climate change impacts on the river flow regimes under CMIP5 RCP scenarios in the westerlies dominated belt, northern Pakistan. Atmos Res 227:233–248
4. Araya-Osses D, Casanueva A, Román-Figueroa C, Uribe JM, Paneque M (2020) Climate change projections of temperature and precipitation in Chile based on statistical downscaling. Clim Dyn 54(9):4309–4330
5. Bayatvarkeshi M, Zhang B, Fasihi R, Adnan RM, Kisi O, Yuan X (2020) Investigation into the effects of climate change on reference evapotranspiration using the HadCM3 and LARS-WG. Water 12(3):666
6. Bodman RW, Karoly DJ, Dix MR, Harman IN, Srbinovsky J, Dobrohotoff PB, Mackallah C (2020) Evaluation of CMIP6 AMIP climate simulations with the ACCESS-AM2 model. J South Hemisphere Earth Syst Sci 70(1):166–179
7. Boudiaf B, Dabanli I, Boutaghane H, Şen Z (2020) Temperature and precipitation risk assessment under climate change effect in northeast Algeria. Earth Syst Environ 4(1):1–14
8. Brusco MJ, Steinley D (2007) A comparison of heuristic procedures for minimum within-cluster sums of squares partitioning. Psychometrika 72(4):583–600
9. Chang J, Wang G, Mao T (2015) Simulation and prediction of suprapermafrost groundwater level variation in response to climate change using a neural network model. J Hydrol 529:1211–1220
10. Chen Y, Song L, Liu Y, Yang L, Li D (2020) A review of the artificial neural network models for water quality prediction. Appl Sci 10(17):5776
11. Chitsazan M, Rahmani G, Neyamadpour A (2015) Forecasting groundwater level by artificial neural networks as an alternative approach to groundwater modeling. J Geol Soc India 85(1):98–106
12. Coppola EA Jr, Rana AJ, Poulton MM, Szidarovszky F, Uhl VW (2005) A neural network model for predicting aquifer water level elevations. Groundwater 43(2):231–241
13. Daliakopoulos IN, Coulibaly P, Tsanis IK (2005) Groundwater level forecasting using artificial neural networks. J Hydrol 309(1–4):229–240
14. Derbela M, Nouiri I (2020) Intelligent approach to predict future groundwater level based on artificial neural networks (ANN). Euro-Mediterranean J Environ Integr 5(3):1–11
15. Di Luca A, Pitman AJ, de Elía R (2020) Decomposing temperature extremes errors in CMIP5 and CMIP6 models. Geophys Res Lett 47(14):e2020GL088031

16. Di Nunno F, Granata F (2020) Groundwater level prediction in Apulia region (Southern Italy) using NARX neural network. Environ Res 190:110062
17. Eyring V, Bony S, Meehl GA, Senior CA, Stevens B, Stouffer RJ, Taylor KE (2016) Overview of the Coupled Model Intercomparison Project Phase 6 (CMIP6) experimental design and organization. Geosci Model Dev 9(5):1937–1958
18. Ghazi B, Jeihouni E, Kalantari Z (2021) Predicting groundwater level fluctuations under climate change scenarios for Tasuj plain, Iran. Arab J Geosci 14(2):1–12
19. Guo D, Wang H (2016) Comparison of a very-fine-resolution GCM with RCM dynamical downscaling in simulating climate in China. Adv Atmos Sci 33(5):559–570
20. Gupta V, Singh V, Jain MK (2020) Assessment of precipitation extremes in India during the 21st century under SSP1-1.9 mitigation scenarios of CMIP6 GCMs. J Hydrol 590:125422
21. Hamidi M, Sabbagh-Yazdi SR (2008) Modeling of 2D density-dependent flow and transport in porous media using finite volume method. Comput Fluids 37(8):1047–1055
22. Hasda R, Rahaman MF, Jahan CS, Molla KI, Mazumder QH (2020) Climatic data analysis for groundwater level simulation in drought prone Barind Tract, Bangladesh: Modelling approach using artificial neural network. Groundw Sustainable Dev 10:100361
23. Hassan Z, Shamsudin S, Harun S (2014) Application of SDSM and LARS-WG for simulating and downscaling of rainfall and temperature. Theoret Appl Climatol 116(1):243–257
24. Hewitson BC, Crane RG (1996) Climate downscaling: techniques and application. Climate Res 7(2):85–95
25. IPCC (2014) In: Team RK, Pachauri, Meyer LA (eds) Climate Change 2014: Synthesis Report. Contribution of Working Groups I, II and III to the Fifth Assessment Report of the Intergovernmental Panel on Climate Change. IPCC, Geneva, Switzerland, p 151. Core Writing
26. Konapala G, Mishra AK, Wada Y, Mann ME (2020) Climate change will affect global water availability through compounding changes in seasonal precipitation and evaporation. Nat Commun 11(1):1–10
27. Li SY, Miao LJ, Jiang ZH, Wang GJ, Gnyawali KR, Zhang J, Zhang H, Fang K, He Y, Li C (2020) Projected drought conditions in Northwest China with CMIP6 models under combined SSPs and RCPs for 2015–2099. Adv Clim Change Res 11(3):210–217
28. Ligotin VA, Savichev OG, Makushin JV (2010) The long-term changes of seasonal and annual levels and temperature of ground waters of the top hydro dynamical zone in Tomsk area. Geoecology 13(1):23–29 (in Russian)
29. MacQueen J (1967) Some methods for classification and analysis of multivariate observations. In Proceedings of the fifth Berkeley symposium on mathematical statistics and probability 1(14):281–297
30. Maharjan M, Aryal A, Talchabhadel R, Thapa BR (2021) Impact of Climate Change on the Streamflow Modulated by Changes in Precipitation and Temperature in the North Latitude Watershed of Nepal. Hydrology 8(3):117
31. Maier HR, Dandy GC (1997) Determining inputs for neural network models of multivariate time series. Computer-Aided Civ Infrastruct Eng 12(5):353–368
32. Moghaddam HK, Moghaddam HK, Kivi ZR, Bahreinimotlagh M, Alizadeh MJ (2019) Developing comparative mathematic models, BN and ANN for forecasting of groundwater levels. Groundw

Sustainable Dev 9:100237

33. Mohanty S, Jha MK, Kumar A, Sudheer KP (2010) Artificial neural network modeling for groundwater level forecasting in a river island of eastern India. Water Resour Manage 24(9):1845–1865
34. Nasiri M, Moghaddam HK, Hamidi M (2021) Development of multi-criteria decision making methods for reduction of seawater intrusion in coastal aquifers using SEAWAT code. J Contam Hydrol 242:103848
35. Natarajan N, Sudheer C (2020) Groundwater level forecasting using soft computing techniques. Neural Comput Appl 32(12):7691–7708
36. Nie S, Fu S, Cao W, Jia X (2020) Comparison of monthly air and land surface temperature extremes simulated using CMIP5 and CMIP6 versions of the Beijing Climate Center climate model. Theoret Appl Climatol 140(1):487–502
37. Nover DM, Witt JW, Butcher JB, Johnson TE, Weaver CP (2016) The effects of downscaling method on the variability of simulated watershed response to climate change in five US basins. Earth Interact 20(11):1–27
38. O'Neill BC, Kriegler E, Ebi KL, Kemp-Benedict E, Riahi K, Rothman DS, van Ruijven BJ, van Vuuren DP, Birkmann J, Kok K, Levy M (2017) The roads ahead: Narratives for shared socioeconomic pathways describing world futures in the 21st century. Glob Environ Change 42:169–180
39. Priestley MD, Ackerley D, Catto JL, Hodges KI, McDonald RE, Lee RW (2020) An Overview of the Extratropical Storm Tracks in CMIP6 Historical Simulations. J Clim 33(15):6315–6343
40. Racsko P, Szeidl L, Semenov M (1991) A serial approach to local stochastic weather models. Ecol Model 57(1–2):27–41
41. Rajaee T, Ebrahimi H, Nourani V (2019) A review of the artificial intelligence methods in groundwater level modeling. J Hydrol 572:336–351
42. Roy DK, Barzegar R, Quilty J, Adamowski J (2020) Using ensembles of adaptive neuro-fuzzy inference system and optimization algorithms to predict reference evapotranspiration in subtropical climatic zones. J Hydrol 591:125509
43. Semenov MA, Barrow EM (1997) Use of a stochastic weather generator in the development of climate change scenarios. Clim Change 35(4):397–414
44. Sha J, Li X, Wang ZL (2019) Estimation of future climate change in cold weather areas with the LARS-WG model under CMIP5 scenarios. Theoret Appl Climatol 137(3):3027–3039
45. Sharma P, Madane D, Bhakar SR (2021) Monthly streamflow forecasting using artificial intelligence approach: a case study in a semi-arid region of India. Arab J Geosci 14(22):1–10
46. Shen C (2018) A transdisciplinary review of deep learning research and its relevance for water resources scientists. Water Resour Res 54(11):8558–8593
47. Srivastava A, Grotjahn R, Ullrich PA (2020) Evaluation of historical CMIP6 model simulations of extreme precipitation over contiguous US regions. Weather and Climate Extremes 29:100268
48. Szidarovszky F, Coppola EA Jr, Long J, Hall AD, Poulton MM (2007) A hybrid artificial neural network-numerical model for ground water problems. Groundwater 45(5):590–600
49. Tabari H (2020) Climate change impact on flood and extreme precipitation increases with water availability. Sci Rep 10(1):1–10

50. Tan ML, Yusop Z, Chua VP, Chan NW (2017) Climate change impacts under CMIP5 RCP scenarios on water resources of the Kelantan River Basin, Malaysia. Atmos Res 189:1–10
51. Taormina R, Chau KW, Sethi R (2012) Artificial neural network simulation of hourly groundwater levels in a coastal aquifer system of the Venice lagoon. Eng Appl Artif Intell 25(8):1670–1676
52. Thorne KM, Elliott-Fisk DL, Freeman CM, Bui TV, Powelson KW, Janousek CN, Buffington KJ, Takekawa JY (2017) Are coastal managers ready for climate change? A case study from estuaries along the Pacific coast of the United States. Ocean & Coastal Management 143:38–50
53. Warnatzsch EA, Reay DS (2019) Temperature and precipitation change in Malawi: Evaluation of CORDEX-Africa climate simulations for climate change impact assessments and adaptation planning. Sci Total Environ 654:378–392
54. Wilby RL, Wigley TM (1997) Downscaling general circulation model output: a review of methods and limitations. Prog Phys Geogr 21(4):530–548
55. Williams KD, Copsey D, Blockley EW, Bodas-Salcedo A, Calvert D, Comer R, Davis P, Graham T, Hewitt HT, Hill R, Hyder P (2018) The Met Office global coupled model 3.0 and 3.1 (GC3. 0 and GC3. 1) configurations. J Adv Model Earth Syst 10(2):357–380
56. Xin X, Wu T, Zhang J, Yao J, Fang Y (2020) Comparison of CMIP6 and CMIP5 simulations of precipitation in China and the East Asian summer monsoon. Int J Climatol 40(15):6423–6440
57. Yan T, Bai J, Arsenio T, Liu J, Shen Z (2019) Future climate change impacts on streamflow and nitrogen exports based on CMIP5 projection in the Miyun Reservoir Basin, China. Ecohydrol Hydrobiol 19(2):266–278
58. Yoon H, Jun SC, Hyun Y, Bae GO, Lee KK (2011) A comparative study of artificial neural networks and support vector machines for predicting groundwater levels in a coastal aquifer. J Hydrol 396(1–2):128–138
59. Zhang Y, You Q, Chen C, Ge J (2016) Impacts of climate change on streamflows under RCP scenarios: A case study in Xin River Basin, China. Atmos Res 178:521–534
60. Zhao L, Dai T, Qiao Z, Sun P, Hao J, Yang Y (2020) Application of artificial intelligence to wastewater treatment: a bibliometric analysis and systematic review of technology, economy, management, and wastewater reuse. Process Saf Environ Prot 133:169–182

Figures

Figure 1

Location of the study area in the map of Iran and the location of piezometer wells in the aquifer

Figure 2

Comparison of Minimum and maximum temperature average and precipitation of base (2000-2019) and future (2021-2040) under 2 scenarios SSP2-4.5 and SSP5-8.5: (a) minimum temperature, (b) maximum temperature, (c) precipitation

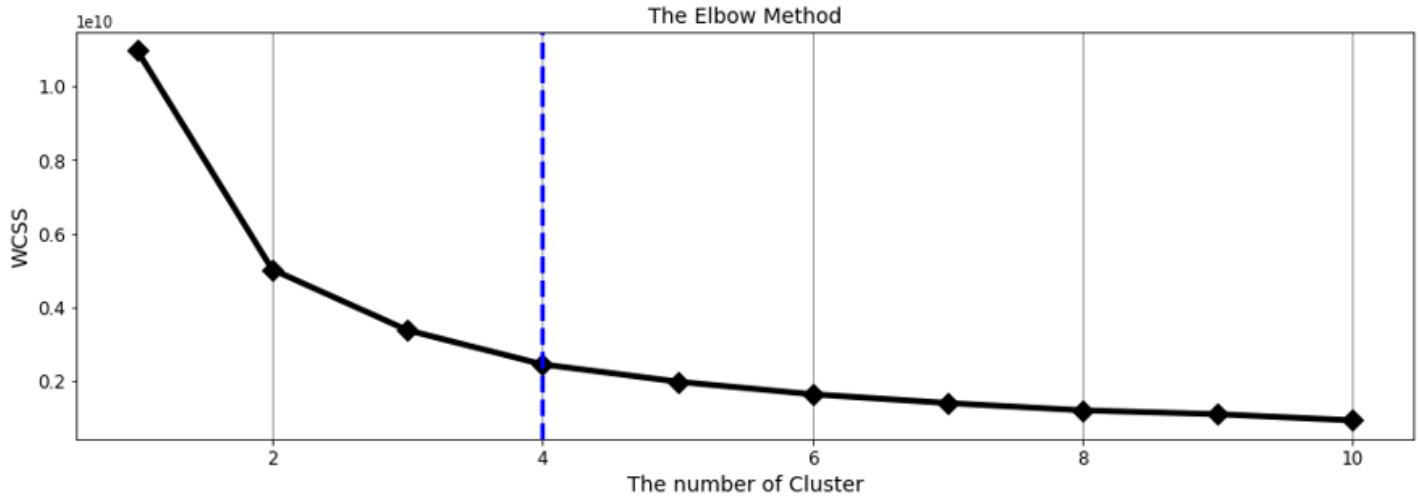

Figure 3

Clustering by Elbow method

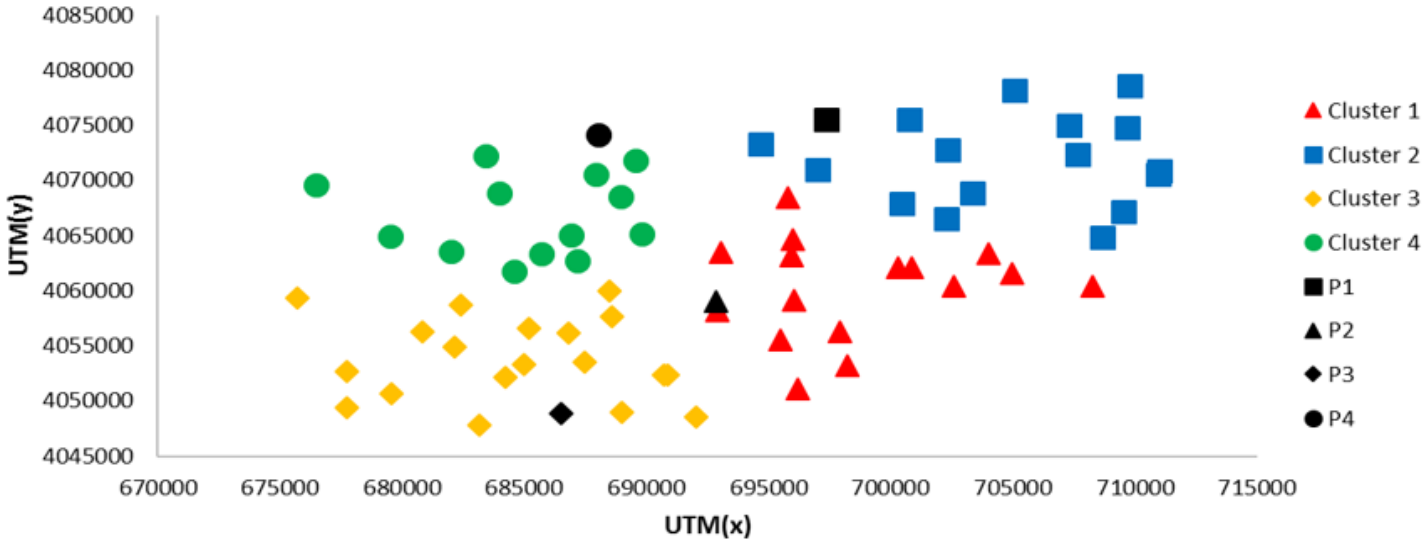

Figure 4

Clustering of groundwater Observation wells and the positioning of representative piezometric wells (P1-P4) on Sari-Neka region

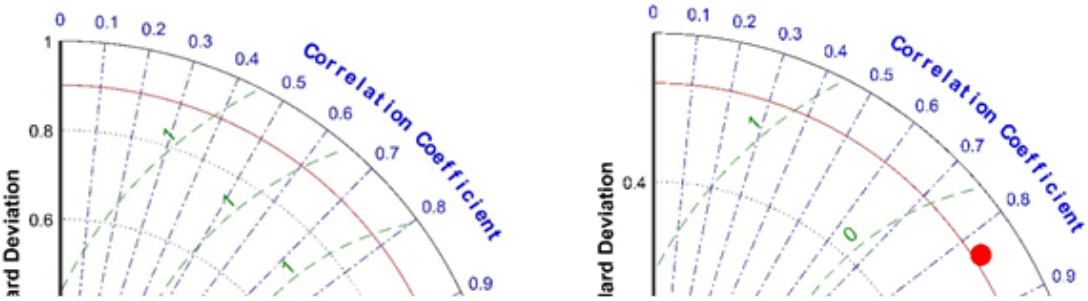

Figure 5

Performance of the artificial neural network based on Taylor diagram

Figure 6

Groundwater level predicted under climate scenarios (SSP2-4.5 & SSP5-8.5) for 2021-2040